IJPMG-International Journal of Physical Modelling in Geotechnics 1(2001) : 09-24

CENTRIFUGE MODELLING OF INJECTION NEAR TUNNEL LINING

S.W. LEE[i], M.D. BOLTON[ii], R.J. MAIR[iii], T. HAGIWARA[iv], K. SOGA[v] and G.R. DASARI[vi]

ABSTRACT

Centrifuge modelling was carried out to simulate the effect of compensation grouting on segmental tunnel lining and ground surface movement in dry sand. Two types of injection were investigated, namely strip injection and multi-point simultaneous injection. For strip injection, the investigated parameters are injection depth, injection distance to tunnel crown (separation), and injection width. The surface heave and lining deformation are found to follow the ratios of injection depth/injection width, and separation/injection width, respectively. To predict the ultimate uplift resistance of soil, two failure mechanisms are proposed for dense and loose sand conditions. In addition, a simple grout pressure transfer mechanism is also suggested to clarify the relationship between the maximum lining deformation and the parameters investigated. The multi-point simultaneous injection tests were conducted to investigate the effect of distributing the injection area. It was found that the sparseness of the injection points has brought beneficial effect to the surface heave and to the lining deformation. In all tests, dense sand shows dilation while loose sand undergoes compression as injected volume increases.

Key words: dense and loose sand, grouting pressure, grouting volume, lining deformation, surface heave

INTRODUCTION

Compensation grouting, the term introduced by Mair and Hight (1994), is a novel technique employed to control ground settlement during tunnelling. Grout is injected at an elevation between the tunnel crown and overlying building foundations to compensate for stress relief and ground loss induced by tunnel excavation. In recent applications, grout injection is carried out simultaneously with tunnelling so that no building settlements are created at the very beginning. This contrasts with previous applications where buildings are first allowed to settle and then compensation grouting is used to jack up the structures. Compensation grouting is best applied in concert with the Observation Method proposed by Peck. (1969). The amount and location of compensation grouting operations should be ascertained in accordance with the observed behaviour of both the ground and the structure, and should be targeted at ensuring that pre-determined limits on acceptable settlement are not approached. Careful interpretations of monitoring data are vital for the successful control of grouting operations in response to observations. In general, there are three types of grouting process used in compensation grouting, namely compaction grouting used in cohesionless soils, fracture grouting used in cohesive soils, and intrusion grouting which is most suitably applied in granular soils with high permeability so that the grout can readily bleed. As this paper discusses injection in dry sand, the literature background of compensation grouting is focussed on compaction grouting.

The use of compaction grouting may be traced back to the "mud-jacking" technique, originating in California in the 1930s, where soil-cement grout was used to raise sagging pavements (Brown and Warner, 1973). Over the years it has been utilised to raise other structures, and for soil improvement. Most recently, contractors have started using it to control ground and buildings movements during tunnelling works. Compaction grouting is different from permeation grouting, as the grout does not enter soil pores. High viscosity, stiff, or low slump paste is injected into the ground to form an approximately columnar or spherical "bulb". Soils surrounding the injection point are displaced and, if loose, may be compacted, by the high grouting pressure and injected grout volume. It should be most effective if used in cohesionless soils. Several factors govern the effectiveness of compaction grouting (Rubright and Welsh, 1993), namely injection pressures, injection volume, injection rate, injection sequence, injection point spacing, surface heave, soil condition, and grout material.

i) Research student, Geotechnical Group, Cambridge University Engineering Department, Trumpington Street, CB2 1PZ, U.K..
ii) Professor of Soil Mechanics and Director of Schofield Centrifuge Centre, ditto.
iii) Professor of Geotechnical Engineering, ditto.
iv) Research engineer, Nishimatsu Construction Co. Ltd., Japan.
v) Lecturer, University of Cambridge.
vi) Lecturer, Department of Civil Engineering, National University of Singapore.
Manuscript was received for review on May 18, 2000.

Baker et al. (1983) reported the successful use of compaction grouting for the Bolton Hill Tunnel, Baltimore, USA. Compaction grouting reduced the volume of the surface settlement trough, V_s above the first and second tunnels from 2 ft^3/ft (0.19m^3/m) to 0.4 ft^3/ft (0.04m^3/m) and 0.2 ft^3/ft (0.019m^3/m), respectively. Below the grout bulbs, settlements would be increased as the grout re-compacted loosened soil over the tunnel and caused downward movement of tunnel lining. Zeigler and Wirth (1982) also commented on the same tunnelling project. They reported that grout pressures were limited to 2800 kPa (400 psi) after it was found that pressures of 3500 kPa (500 psi) were enough to deflect the steel linings until they became jammed in the tail of the shield. In one instance undesirable heave of a concrete basement floor was recorded due to excessive grout pressure in a bulb 6 m below the basement floor. It follows that grouting pressure must be suitably controlled so that it does not excessively deform the tunnel lining below nor create excessive heave above.

Fracture grouting involves the use of low viscosity grout or relatively fluid cement / bentonite grout to split open clayey ground and to form fissure planes along which the grout flows. This technique has proven its effectiveness at St. Clair River Tunnel, Ontario, Canada (Drooff et al., 1995) and Redcross Way, London (Linney and Essler, 1994).

Intrusion grouting also named "pressure filtration" uses grout which is fluid but with high solids content, and is generally used in sands and gravels. The grout is mixed to bleed rapidly so that water is lost into the surrounding ground and the solids are deposited close to the point of injection. Harris et al. (1994) gave an example of the successful use of intrusion grouting implemented at Waterloo Station, London.

Based on the case histories presented above, there is no doubt that compensation grouting can create surface heave provided the technique is used correctly. However, recent urban tunnelling work frequently requires the grouting injections to be carried out close to the tunnel lining. This is due to the foundations of existing buildings and subsurface utilities, and to shallow tunnelling where the overburden resistance is small. Previous work on the effects of compensation grouting on tunnel linings or ground movements were based on numerical analysis; Nicholson et al. (1994), Kovacevic et al. (1996), Schweiger and Falk (1998), and Lee et al. (1999). The investigated parameters are the grouting width, grouting depth and the distance of the grouting array above the tunnel crown.

No physical modelling work had been done before to investigate the effects of injection close to a segmental tunnel lining, and corresponding ground surface movements. This paper discusses such an investigation involving the Cambridge University Geotechnical Group and the Japanese tunnelling contractor, Nishimatsu Construction Co. Ltd.. Parametric studies carried out in the strip injection tests involved parameters: grouting width (B), grouting depth (A), and separation between grouting level and tunnel crown (Y). Multiple-point injection tests investigated the effect of distributing the injection areas. Tests were generally done in dense dry sand, but two selected tests were redone in loose dry sand to clarify the difference between dense and loose sands.

CENTRIFUGE MODELLING

Introduction

Centrifuge testing was carried out at the Schofield Centrifuge Centre (SCC). All tests were in plane strain (2-D) and carried out under 75-g. Figure 1 shows a schematic view of the centrifuge package in a strip injection test. The strong box is made of 10 mm thick aluminium alloy and has internal dimensions of 250 mm depth, 300 mm across the tunnel and 250 mm along the tunnel axis, see Fig. 3. The total height of the sand sample was

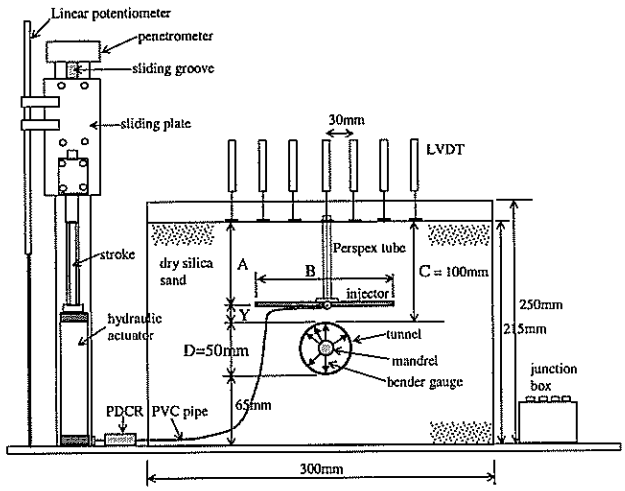

Fig. 1. Schematic view of a strip injection centrifuge model set-up (not to scale)

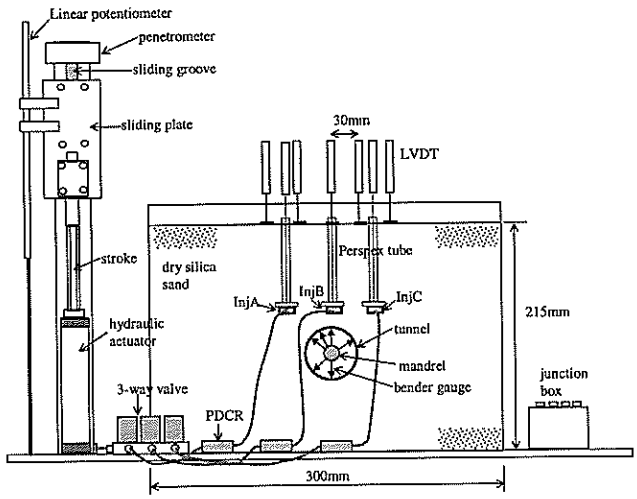

Fig. 2. Schematic view of a multi-point injection centrifuge model set-up (not to scale)

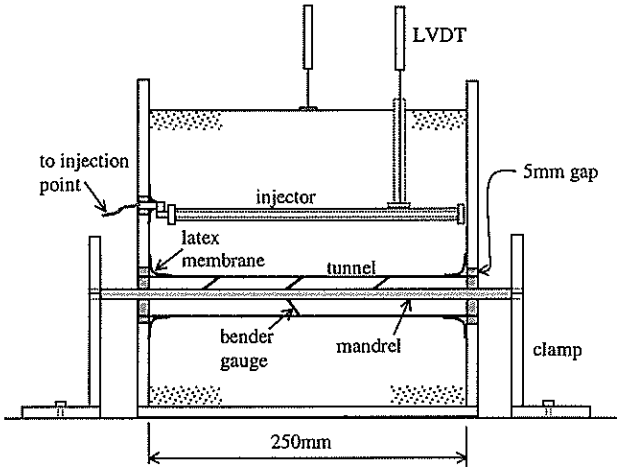

Fig. 3. Side view of a typical centrifuge model set-up (not to scale)

215 mm. The distance from the sand surface to the tunnel crown C was 100 m, the tunnel diameter D was 50 mm and the depth from the tunnel invert to the base of strong box was maintained at 65 mm. Figure 2 is the schematic view for the set-up of a multiple-point injection test.

Sand properties

The centrifuge tests used commercial dry silica sand (Leighton Buzzard), Fraction E - Grade 100/170 - Size 90-150 microns. The D_{10}, D_{50} and D_{60} grain sizes are 0.095, 0.14 and 0.15 mm, respectively. It has a minimum void ratio, e_{min} of 0.65 (γ_{max} = 16.0 kN/m^3) and a maximum void ratio, e_{max} of 1.01 (γ_{min} = 13.3 kN/m^3). The specific gravity G_s is 2.67 and the critical state angle, ϕ_{crit} is 32° (Tan, 1990).

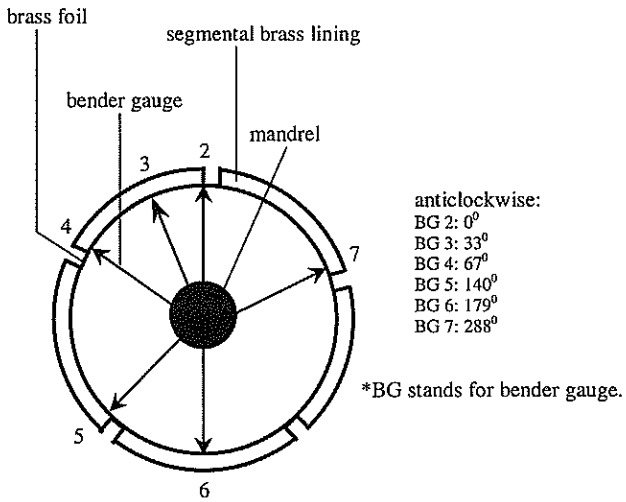

Fig. 4a. Position of bender gauge

Segmental tunnel lining

The tunnel lining was based on a thin brass foil of 0.15 m thickness, see Fig. 4 a. Five brass segmental lining sections with 1.5 mm thickness were then glued onto the brass foil to leave a gap of 2mm between adjacent segments. This is to model the full-scale lining joint where

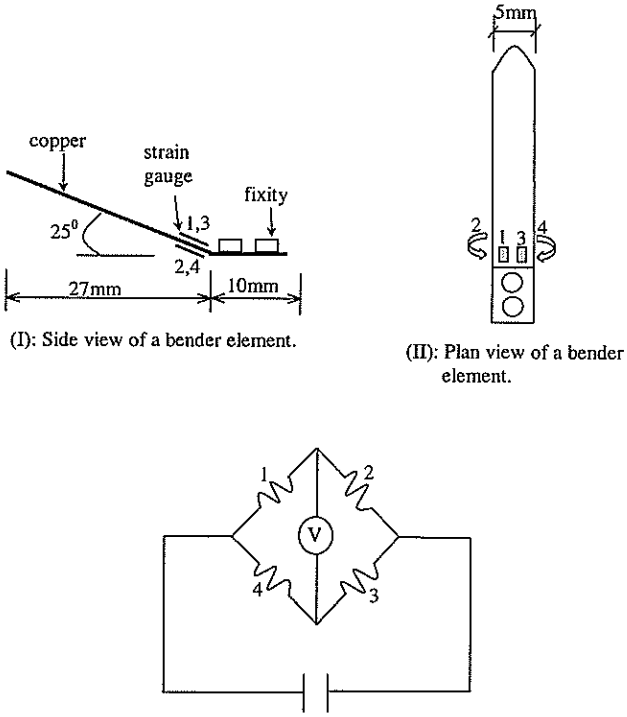

Fig. 4b. The electronic set-up of a bender gauge

the bending stiffness is much reduced compared with the lining segment. The lining ran the full length of the strong box and it was free floating in the sand sample.

Bender gauge

To measure the radial displacement of the tunnel lining, a mandrel with eight bender gauges fixed on it was inserted into the tunnel. Two bender gauges were fixed at one-quarter and three-quarters length at the tunnel crown to check the uniformity of deformations along the tunnel axis, see Fig. 3. In the middle section of the tunnel, six bender gauges were used, pointing to the edge or to the middle section of 4 of the 5 segments, see Fig. 4a. Figure 4b shows the electronic set-up of a bender gauge. It was made of thin beryllium copper and carried two pairs of strain gauges on the top and the bottom at its fixity end. One pair of strain gauges measured the tension deformation and the other one measured the compression deformation. It adopted the full Wheatstone Bridge system so that it was not subject to the temperature effect. The excitation voltage was 5V and its output was amplified 100 times via a junction box. The sharpened tip was to attain a point contact with the tunnel lining. These gauges have a coefficient of correlation or R between 0.9984 and 0.9998, and a resolution of 0.005 mm. An example of the bender gauge calibration charts is shown in Fig. 4c. They were slightly compressed inside the lining before the centrifuge testing so that both outward and inward displacements can be recorded. The mandrel was fixed in position through two end clamps.

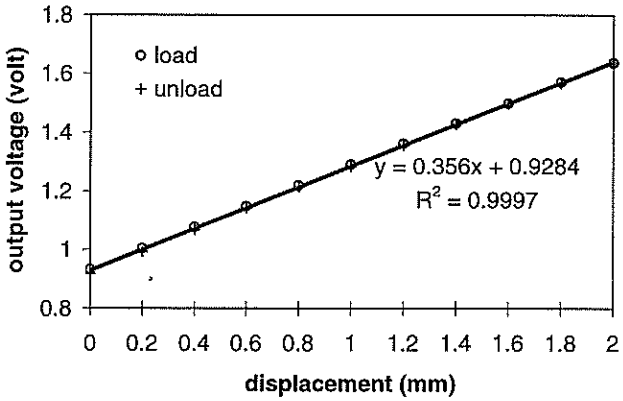

Fig. 4c. An example (BG2) of bender gauge calibration charts

Injector

An injector was used to simulate the compaction grouting. It was made of a copper tube squashed flat to form a tabular strip of thickness 4 mm. Drainage holes were drilled at both ends for fluid (water) injection and de-airing purpose, and also on the top and bottom of the strip surface. Then a tight fitting rubber sleeve of 1mm thickness was slid onto the tabular strip and clamped at both ends. When water was injected into the tabular strip it would flow out from the top and bottom pre-drilled holes, expanding the wrapping rubber sleeve both upward and downward rather in the fashion of a pressuremeter. This expansion mimics compaction grouting. The injector was placed on the centreline above the tunnel, and running its full length so as to comply with the plane strain condition. Three different widths (30, 55 and 80 mm) of injector were used in strip injection tests. For multiple-points injection tests, injector widths of 10 and 20 mm were employed. Figure 5 shows the five different widths of injectors.

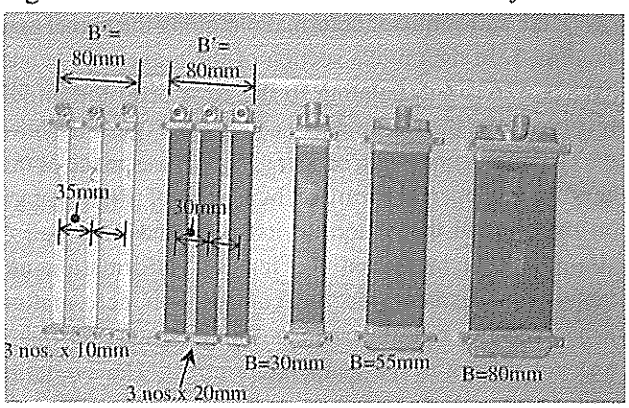

Fig. 5. Multi-point and strip injectors used in centrifuge testing

Injection system

A hydraulic cylinder was used to store the injection fluid (water) which was expelled using an electrically controlled linear actuator, see Fig. 1 and Fig. 2. Hence the rate of injection was controlled precisely. A linear potentiometer was attached to the sliding plate to record the travel of the actuator stroke which corresponds to the injected volume via the constant cylinder area. A pressure transducer was connected to the outlet of the cylinder to measure the fluid pressure within the system, which had been de-aired beforehand. In the multiple-point injection tests, see Fig. 2, a 3-way valve controls the independent injection to the three injectors. Each injector was allocated its own pressure transducer.

Model preparation

In preparing the dense sand model, sand was vibrated in layers as the model was built up to achieve the densest possible relative density and the good bedding of sand against the tunnel. First the sand was poured up to the tunnel invert level and vibrated, see Fig. 3. Then the tunnel was placed. There are two pre-drilled holes of 60 mm diameter through the sides of the strong box to provide access to the tunnel. Two circular pieces of latex membrane with a small hole in the centre were slid onto the tunnel lining at both ends. They were stuck to the sides of strong box with silicone grease so as to seal off the annular gap of 5 mm around the lining. At this stage the tunnel was held in position using two O-rings plugged into the holes on the two sides of the strong box. With this arrangement the lining was virtually free floating once the O-rings were removed, as the silicone grease on the latex membrane offers negligible frictional resistance. After this, more sand was poured and vibrated up to the injector level. The injector was also free floating in the model, adopting the same fixity approach used in tunnel. A vertical perspex tube seated on the injector could receive an Linear Variable Differential Transducer (LVDT) needle to measure the lift of the rubber membrane after injection. Then sand was poured and vibrated up to the required level. More LVDTs were placed on the sand surface to measure the surface heave. The relative density, I_D of sand achieved in the tests was 90% (corresponding to a dry density of 15.83 kN/m^3) with test-to-test variation in I_D of ± 4%.

Sand internal friction angle

Bolton (1986, 1987) suggests that the peak angle of internal friction of sand can be estimated within one or two degrees using

$$\phi_{max} = \phi_{crit} + A[I_D I_C - 1] \quad (1)$$

where A in Equation (1) is an index and can be taken as 5° in plane strain, and the relative crushability I_C can be taken as a maximum of 5 at low stress levels reducing at higher stress levels to $\ln(\sigma_c/p')$ where σ_c is an aggregate crushing stress (circa 20, 000 kPa) and p' is the mean effective stress at failure. In these tests the major principal stress at failure is roughly twice the overburden pressure (from 1.5 to 3 times) at the injector, see Fig. 7. So the mean effective stress near the injector will be about

1.2 times the overburden pressure, and taking two-thirds depth as representative of the heave mechanism, the mean effective stress at failure will be about 0.8 times overburden pressure, or about 70 kPa. It follows that the limiting value I_C = 5 will apply in this case, giving ϕ_{max} = 49.5° for a relative density I_D = 0.9.

In order to prepare a centrifuge model with sand as loose as possible, it is necessary to avoid compaction by subsequent vibration or shock during the loading of the model on the beam centrifuge. Sand was therefore poured while the model was hanging on the centrifuge rotor. To do this, a sand slumping technique was adopted. By positioning the "elephant trunk" hose of the sand hopper very close to the sand surface, sand would have no chance to gain velocity and energy to compact itself as it completely chokes the hose. When the hose is repeatedly lifted, translated and lowered in small steps, the sand slumps out in a succession of loose mounds. The achievable relative density I_D using this technique was on average 27% (corresponding to a dry density of 13.58 kN/m^3). At this density the peak angle of internal friction should be about 33.7° using Equation (1) as before.

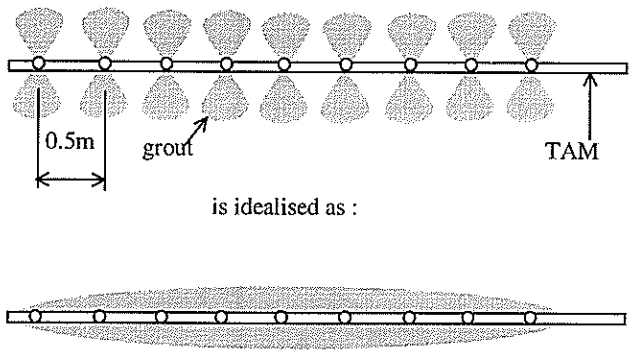

Fig. 6. Idealisation of Strip injection

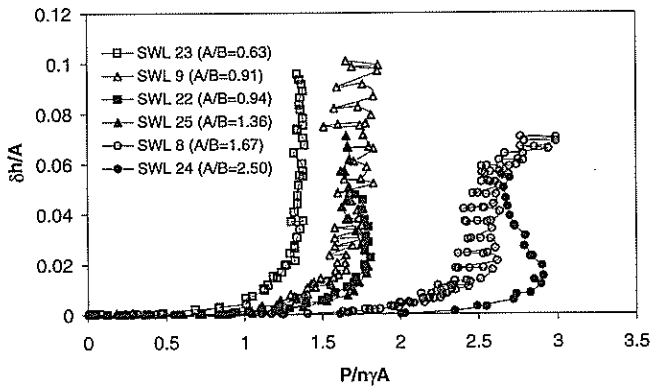

Fig. 7. Centre surface heave over depth ratio δh/A vs. normalised grouting pressure, P/nγA for dense sand tests

In-flight procedure

The beam centrifuge was advanced in 25-g increments up to the test acceleration of 75-g. Ground surface settlement and lining deformation due to the increased g-force were recorded during this period. To make sure that the sand had completely settled, a lapsed period of approximately ten minutes was allocated upon achieving 75-g before making injections. This is essential so that the subsequent lining deformation was due to the injection only. Injection was made in stages so that data could be recorded manually after every injection. In addition to this, the data acquisition software, Labtech Notebook also recorded the instrument readings automatically. After injecting the pre-determined volume of fluid, the test acceleration was brought down in 25-g decrements.

This paper reports ten centrifuge test results from a total of twenty-one tests conducted. Table 1 and Table 2 detail the relevant tests grouting geometry, the sand condition and the type of injections.

Table 1. Details of strip injection tests

Test	B (mm)	Y (mm)	A (mm)	Sand Condition
SWL 8	30	50	50	Dense
SWL 9	55	50	50	Dense
SWL 22	80	25	75	Dense
SWL 23	80	50	50	Dense
SWL 24	30	25	75	Dense
SWL 25	55	25	75	Dense
SWL 28	55	25	75	Loose

Table 2. Details of multi-point simultaneous injection tests

Test	B (mm)	Y (mm)	A (mm)	Injector c/c spacing, (mm)	Sand Condition
SWL 12	20	25	75	30	Dense
SWL 15	10	25	75	35	Dense
SWL 27	10	25	75	35	Loose

STRIP INJECTION

Introduction

In the field, grouting points are spaced as close as 0.5 m - 1m centres along the Tube-a-Manchette (TAM) and the injected grout bulbs may overlap each other. As such, it may be reasonable to idealise the grouting array as a strip, see Fig. 6. Table 1 summarises the tests investigating strip injection. Seven tests were conducted, six in dense

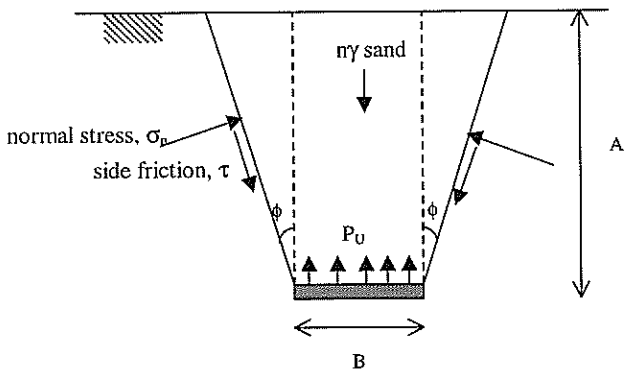

Fig. 8a. Proposed upper bound plastic solution (Mechanism I)

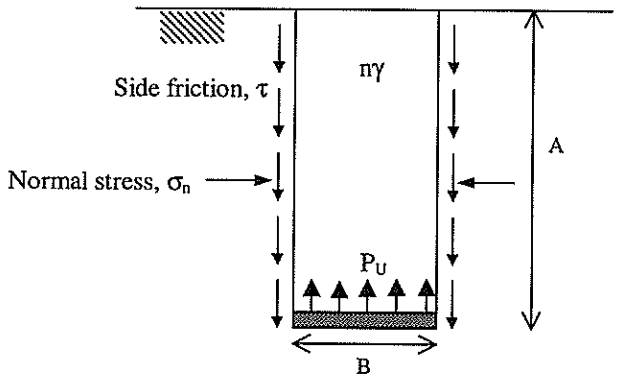

Fig. 8b. Proposed limit equilibrium analysis (Mechanism II)

sand and one in loose sand. Three grouting widths B were used, 30, 55 and 80 mm at injection separations Y of 25 and 50 mm (corresponding to injection depths A of 75 and 50 mm), see Fig. 1.

Ground movement

The centre ground surface heave δh (above the centreline of injector) with respect to grouting pressure P for dense sand tests is shown in Fig. 7. Parameters δh and P in Fig. 7 are normalised by the depth of injector A and overburden pressure nγA, respectively. The trend of surface heave follows the injector depth/width ratio, A/B. Smaller A/B ratio lifts the ground earlier, and hence has smaller ultimate uplift resistance P_U. P_U is reached at δh/A ≈ 0.02-0.03 for all tests. The data of model tests are best presented in terms of normalisation based on physical mechanisms. To predict the ultimate uplift resistance, two failure mechanisms are investigated, see Fig. 8. Mechanism I is an upper bound plastic solution using dilation angle ψ = friction angle φ so that the motion of the soil block is kinematically admissible. Referring to Fig. 8a, the stresses acting on the shear band are σ_n and τ ($\tau = \sigma_n \tan\phi$) but their resultant is purely horizontal and does not contribute to vertical equilibrium. Resolving vertically for the uplifting block,

$$P_U B = \eta\gamma AB + 2(0.5A^2 \tan\phi\, n\gamma)$$

$$\frac{P_U}{\eta\gamma A} = 1 + \frac{A}{B}(\tan\phi) \qquad (2)$$

This correctly over-predicts the six dense sand centrifuge results by setting φ equal to the estimated peak value (49.5°), see Fig. 9a. The variable degree of over-prediction suggests that progressive failure may be responsible for reducing φ on average below ϕ_{max}. Shear bands will form first at the edges of injector and then propagate upwards, so that critical state condition will apply close to the injector at the instant of failure.

Mechanism II is a limit equilibrium analysis which ignores dilation and uses an earth pressure coefficient K multiplied by the pre-existing vertical effective stress σ'_{vo} to permit the calculation of normal stress on the sides of the lifting block. Referring to Fig. 8b, assuming that friction is fully mobilised on the sides of the block, where

$$\sigma_n = \sigma_h = K\sigma'_{vo}$$
$$\tau = K\sigma'_{vo} \tan\phi$$

Resolving vertically for the rectangular block,

$$P_U B = \eta\gamma AB + 2\left(\frac{1}{2}K\eta\gamma A \tan\phi\right) A$$

$$\frac{P_U}{\eta\gamma A} = 1 + \frac{A}{B}(K \tan\phi) \qquad (3)$$

The "skin friction" on the sides of the block is therefore written as $(K\tan\phi)\sigma'_{vo}$ or $\beta\sigma'_{vo}$ using the standard nomenclature for effective stress design of piles. Figure 9a shows that for dense sand ($I_D \approx 90\%$) in the range of geometries tested above, the best fit K value is 0.67 giving β = 0.79 when φ is taken as 49.5°.

Figure 9b shows the single uplift failure for loose sand, in which the final normalised uplift pressure is seen in relation to the prediction of Mechanism I with φ = 33.7°, and Mechanism II with K=0.67 as before and φ = 33.7° giving β = 0.45. The laboratory data lies close to the predicted line of Mechanism II.

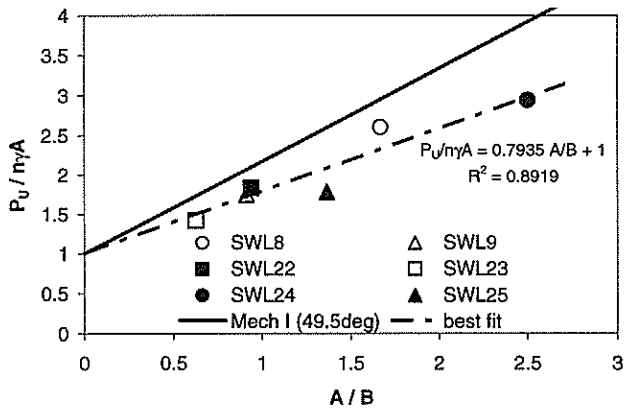

Fig. 9a. Normalised ultimate uplift resistance $P_u/n\gamma A$ vs. injection depth over width ratio A/B for dense sand tests

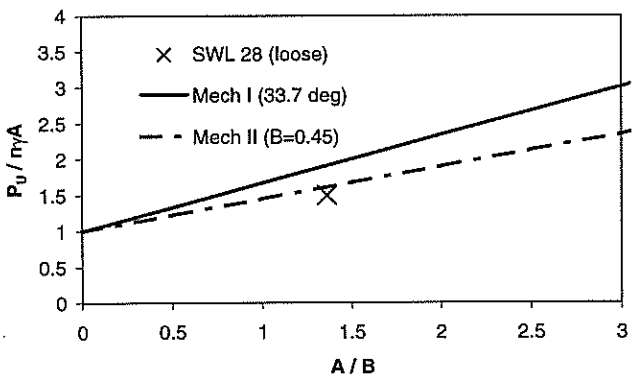

Fig. 9b. Normalised ultimate uplift resistance $P_u/n\gamma A$ vs. injection depth over width ratio A/B for loose sand tests SWL 28

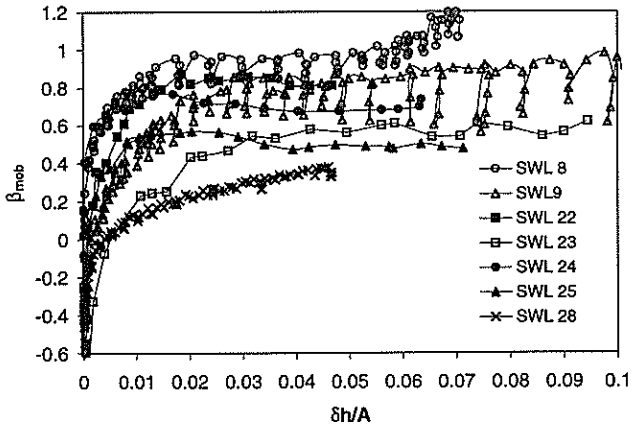

Fig. 9c. Mobilised skin friction, β_{mob} vs. centre surface heave over depth ratio δh/A

Figure 9c shows the mobilised β value (β_{mob}) for all the tests. It can be seen that for the dense sand tests, the maximum β_{mob} varies between 0.6 and 1.0 in the vicinity of β = 0.79 as described above. The variation in β_{mob} might suggest that progressive failure had occurred to different degrees in the different dense sand tests. In loose sand the maximum β_{mob} is 0.38 before reaching the peak point which should have given β = 0.45 as indicated above. Empirically, therefore, grout-zone injections having geometries within the bounds indicated in Table 1 might be regarded as having a peak uplift pressure (average within the grout zone) calculable using Equation (3) with K ≈ 0.67 and taking a value for ϕ consistent with density and stress level.

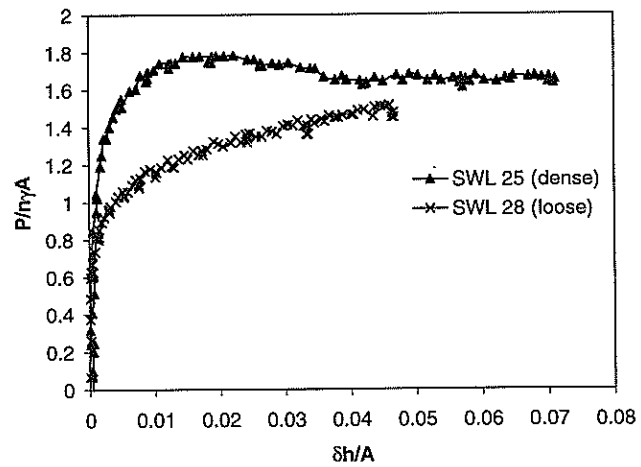

Fig. 10. Normanlised grouting pressure, P/nγA vs. centre surface heave over injection depth ratio, δh/A

Figure 10 shows the normalised grouting pressure P/nγA versus the centre surface heave over injector depth ratio δh/A for tests SWL 25 (dense) and 28 (loose) which have the same grouting geometry but different sand densities. This figure can be read as an ordinary soil stress-strain curve where dense sand demonstrates strain hardening to peak at a "strain level" δh/A ≈ 0.02 and then strain softening to the critical state point; loose sand, as expected, shows only strain hardening before approaching a critical state.

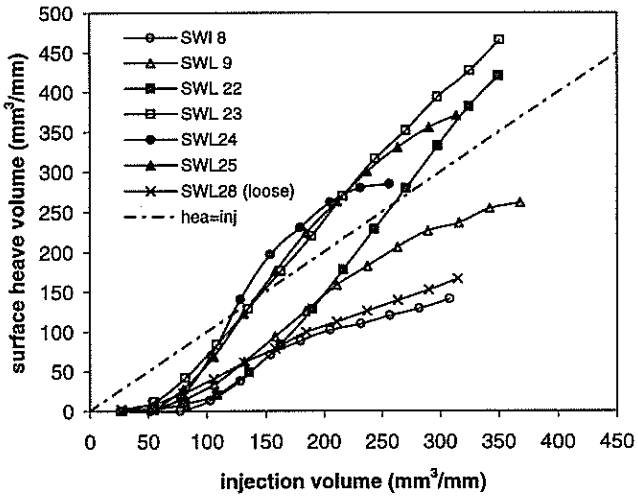

Fig. 11. Surface heave volume vs. injection grout volume

Figure 11 compares the surface heave volume with the injected grout volume. The volume is expressed in term of mm^3/mm as this is a plane strain study. The surface heave volume was determined from the integration of area beneath the surface heave points. If the lateral extent of surface heave was beyond the LVDTs range, physical observation after the test determined the boundary of the integration points. Figure 12 shows an example of surface heave after a test, in this case test SWL 24. The longitudinal extent of surface heave was always corresponding to the effective length l ≈200mm) of the injector used based on the physical observations after each test. The injector end effect arising from the use of end clamps was about 7 mm at each end. So, the uncertainty of the measured surface heave volume was less than 7 %.

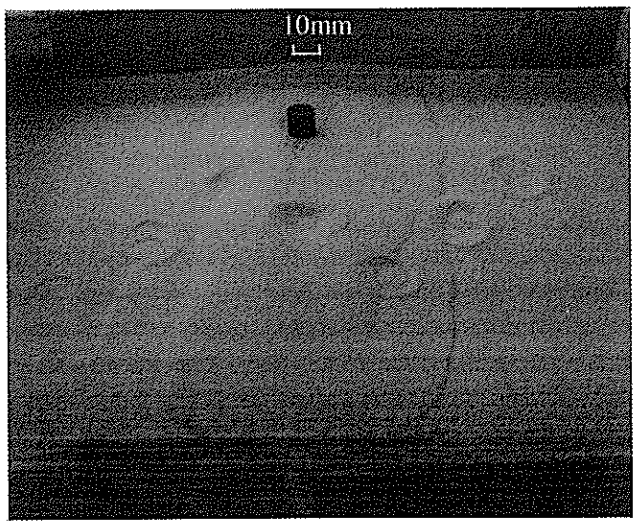

Fig. 12. Physical observation of surface heave after test SWL24

Figure 11 shows that for tests SWL 22, 23, 24 and 25 the heave volume is more than the injected volume after

overcoming the ultimate uplift resistance P_U. This extra volume of heave is due to the dilation behaviour of dense sand. The injected volume at failure (vol_U) of about 100 to 150 mm^3/mm, and the corresponding P_U point can be read from Fig. 13. For tests SWL 8 and 9 only, Fig. 13 shows that grouting pressures relax after every injection, especially after overcoming the uplift resistance. Furthermore, Fig. 11 shows that the injected volume in these tests is more than the heave volume even though the sand was as dense as in the other tests and full uplift failure was achieved. This discrepancy is probably due to a very small undetectable leakage, or to the compression of bubbles accidentally left in the hydraulic system. Accordingly, injection volume data in Fig. 11, and 13 for tests SWL 8 and 9 should be treated as an over-estimate.

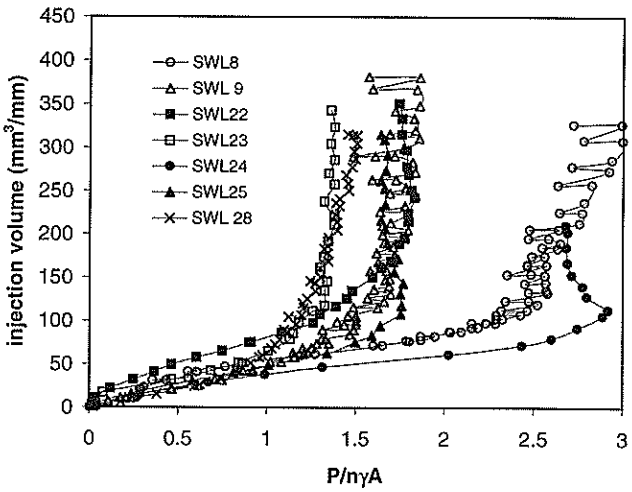

Fig. 13. Injection volume vs. normalised grouting pressure,P/nγA

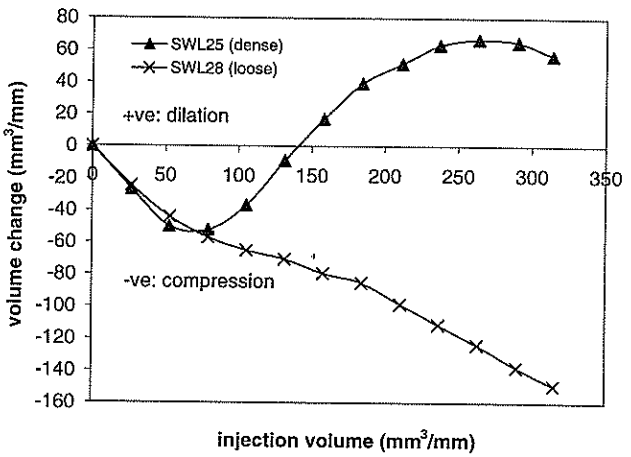

Fig. 14. Volume change (heave volume minus injection volume) vs. injection volume of dense (SWL 25) and loose sand (SWL 28)

Figure 14 distinguishes the dilation and compression behaviour of sand for tests SWL 25 (dense) and 28 (loose) where volume change (heave volume minus injection volume) is plotted against the injection volume. Both tests have the same rate of injection, see Fig. 15. As shown in Fig. 14, test SWL 25 starts to dilate before reaching the vol_U value at about 135 mm^3/mm (determined from Fig. 13). Upon reaching vol_U the dilation rate is the highest. Test SWL 28 in loose sand shows continuous compression with increasing injection volume such that the heave volume is about one half of the injection volume. The curves in Fig. 14 resemble the typical volume change behaviour of dense and loose sand subjected to shearing. In this case, the actual locations of compaction and dilation are presumably distributed around the injector and in the region of shear surfaces from the injector to the soil surface.

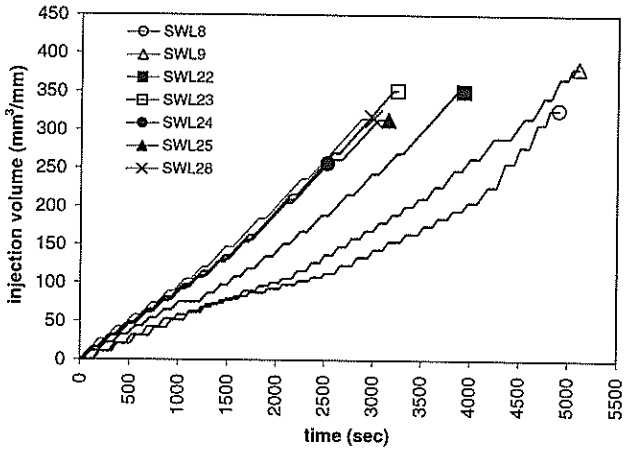

Fig. 15. Rate of injection volume

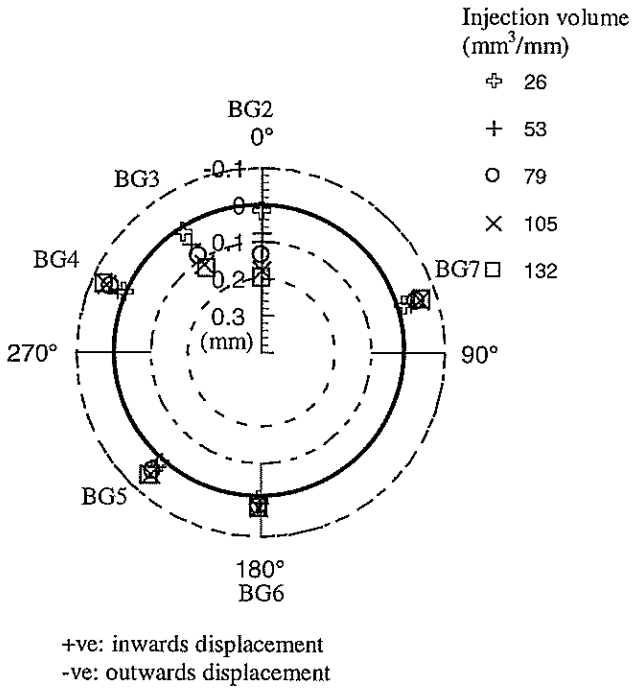

Fig. 16. Polar plot of radial lining deformation δ (mm) for test SWL25

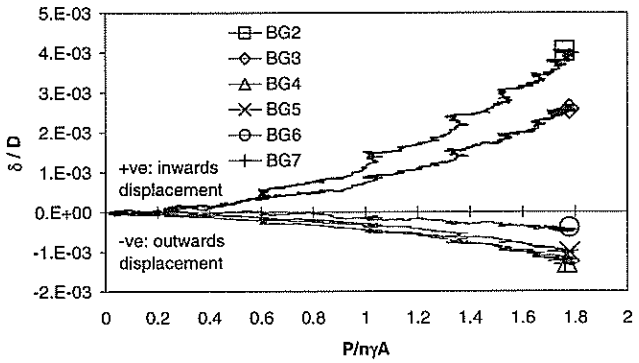

Fig. 17. Normalised lining deformation δ/D vs. normalised grouting pressure P/nγA for test SWL 25

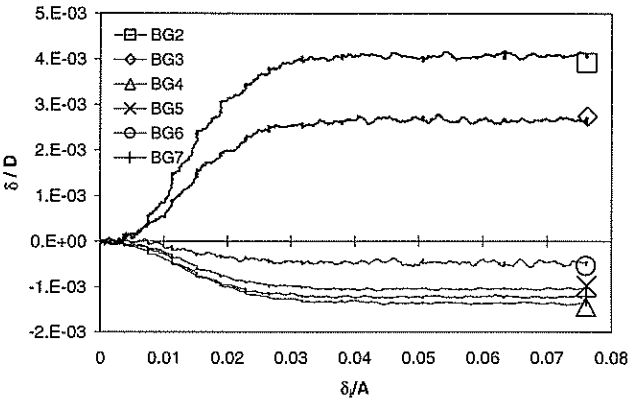

Fig. 18. Normalised lining deformation δ/D vs. injection thickness over depth ratio δ/A for test SWL 25

Lining deformation

Figure 16 shows a typical polar plot of radial lining deformations δ against the injected volume for test SWL 25 on dense sand. In general, the tunnel crown (BG 2) and upper shoulder (BG 3) suffered from inward displacement (compression) while the tunnel shoulder (BG 4 & 7), haunch (BG 5) and invert (BG 6) experienced outward displacement (extension). The small displacement at tunnel invert suggests that the whole tunnel has been slightly pushed down by the grouting pressure above the crown. Figures 17 and 18 show the lining deformations normalised by tunnel diameter δ/D against the normalised grouting pressure P/nγA and the injection thickness per depth ratio δ_i/A, respectively, for test SWL 25. The injection thickness δ_i is defined as injection volume (ml) per area of injector (*l*B). From Fig. 18, it can be seen that the lining ceases to deform after δ_i/A = 0.03 (or 135 mm^3/mm of injection volume). Figure 13 shows that this corresponds to the P_U value for test SWL 25. Further injection of grout does not affect the lining, as the grouting pressure has peaked out. All dense sand tests show the same phenomenon. In test SWL 28 which has the same grouting geometries as test SWL 25 but on loose sand, the lining deformations do not show a sudden cessation, see Fig. 19. This is due to that loose sand continues to strain harden before reaching the ultimate point, as shown in Fig. 13. Among all sensor positions, the tunnel crown always displaced the most in these injections above the crown.

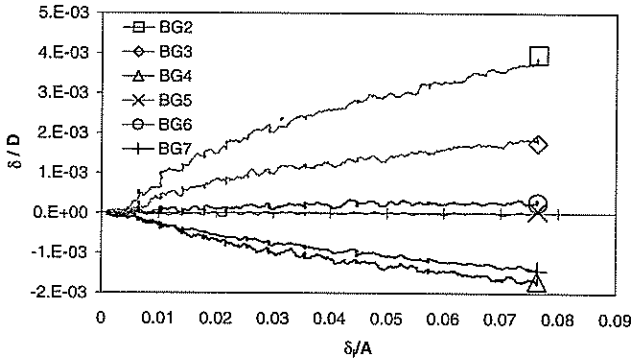

Fig. 19. Normalised lining deformation δ/D vs. injection thickness over depth ratio δ_i/A (SWL 28)

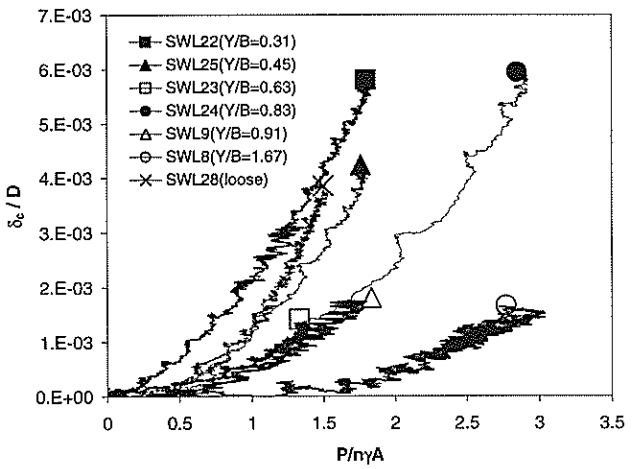

Fig. 20. Normalised tunnel crow deformation δ_c/D vs. normalised grouting pressure P/nγA for strip injection test

Figure 20 shows that tunnel crown deformation δ_c is dependent on injection separation over width ratio Y/B as well as normalised grouting pressure P/nγA. A smaller Y/B ratio, meaning a nearer and wider injection, causes more deformation. Tests SWL 25 (dense) and SWL 28 (loose) show about the same crown deformation until P/nγA is 0.9. After that, the test in loose sand deforms the lining more. This is because of differences in the grouting pressure versus injection volume relationship which will be discussed later when lining deformation is plotted against the injection thickness.

Figure 21 shows the normalised tunnel crown deformation δ_c/D against the injection thickness over depth ratio δ_i/A. For dense sand tests they still, more or less, follow parameter Y/B until δ_i/A is 0.025. After that, some tests like SWL 25 and 23 have overcome the ultimate uplift resistance P_U and the tunnel crown deformation becomes stable.

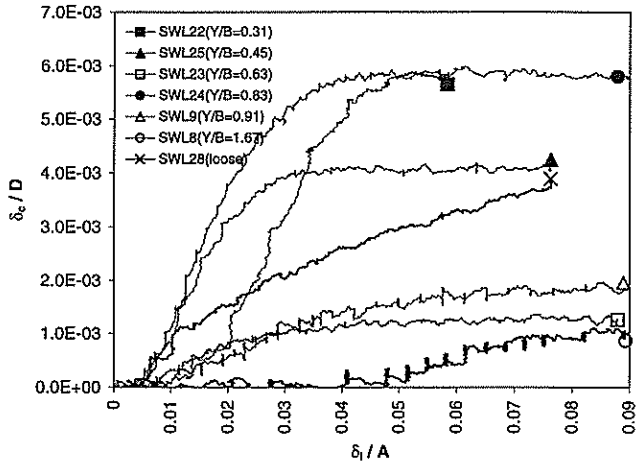

Fig. 21. Normalised tunnel crow deformation δ_c/D vs. injection thickness over depth ratio δ_i/A

Comparing tests SWL 25 (dense) and SWL 28 (loose), referring to Fig. 21, it can be seen that both tests have the same lining deformations up to $\delta_i/A \approx 0.01$ (or 37 mm^3/mm of injection volume). Thereafter, the test in dense sand has a more dramatic increase of lining deformations and reaches the maximum value earlier than in loose sand. As lining deformation depends not only on grouting volume but also grouting pressure, Fig. 13 explains why the lining was distorted in that fashion. Below 37 mm^3/mm of injection volume both tests have similar normalised grouting pressures $P/n\gamma A$. Hence the lining was deformed to the same magnitude. Later, the test in dense sand produces more grouting pressure compared with the loose sand test. This explains the higher rate of lining deformations in dense sand before reaching its P_U at 135 mm^3/mm of injection (or $\delta_i/A = 0.03$). It can therefore be said that grouting in dense sand has more effect on the tunnel lining for the same amount of injected volume, prior to overcoming the ultimate uplift resistance.

A new mechanism is required to organise the data of tunnel deformations, see Fig. 22. The sequence of actions is:

a) the pressure in the injector creates a pressure increment on the tunnel crown.
b) the equilibrium of the tunnel demands reaction pressures around the other tunnel segments.
c) the mobilisation of these reactions demands that the sides of the tunnel move out.
d) the kinematics of the tunnel demands that the crown depresses as the sides move out.

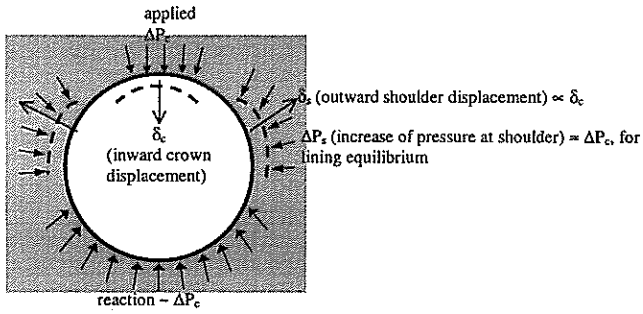

Fig. 22. Structural equilibrium of lining

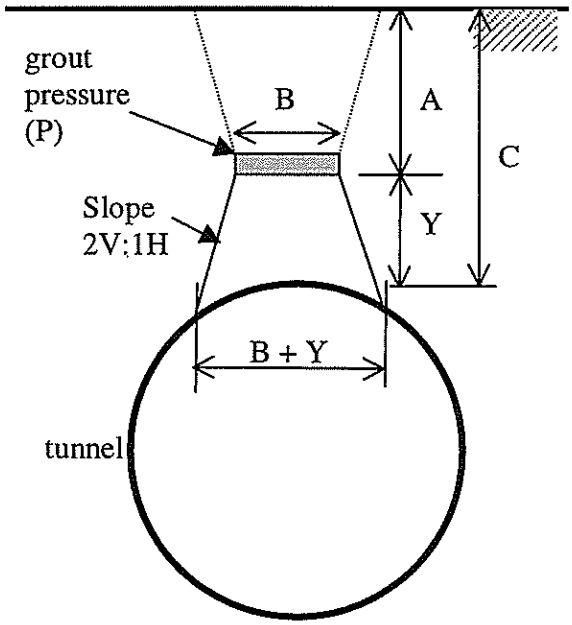

Fig. 23. Transfer of grout pressure to tunnel lining

All that required is a simple model which respects these principles, and which can be used to normalise the raw data. The simplest possible elements are therefore selected. Referring to Figs. 22 and 23, in step (a) the grout pressure is assumed to spread at a slope of 2V:1H so that the increment of pressure at the crown is given by

$$\Delta P_c = P\ B/(B+Y) \quad (4)$$

In step (b) we assume that the segmental tunnel attracts zero bending moments due to the negligible bending resistance at its joints. In that case, a circular tunnel will tend to attract constant radial stresses so that its line of thrust remains at the centre of the segments. Therefore we assume that the pressure increment at the sides of the tunnel.

$$\Delta P_s \approx \Delta Pc \quad (5)$$

In step (c) we invoke ideas of cavity expansion to estimate the outward expansion of the sides

$$\delta_s/D \propto \Delta P_s / G \quad (6)$$

where G is the shear modulus of soil.

And in step (d) we use the idea of a linkage of rigid segments suffering a small distortion to establish a kinematic mechanism in which the crown compression will be proportional to the side extension.

$$\delta_c \propto \delta_s \quad (7)$$

Putting (4), (5), (6) and (7) together we obtain.

$$\delta_c / D \propto \{P / G\} \{B / (B+Y)\} \quad (8)$$

Then taking G to be proportional to the vertical stress at tunnel crown level, nγC, we obtain

$$\frac{\delta_{c,U}}{D} \propto \frac{P_U}{\eta\gamma C} \frac{1}{(1+\frac{Y}{B})} \quad (9)$$

where $\delta_{c,U}$ is the maximum tunnel crown deformation at the ultimate uplift resistance P_U.

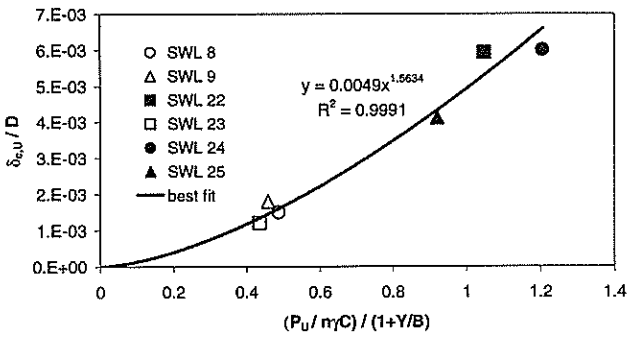

Fig. 24. Normalised maximum tunnel crow deformation δ_c/D versus normalised grouting pressure $(P_u/n\gamma C)$ / (1+Y/B) for dense sand tests

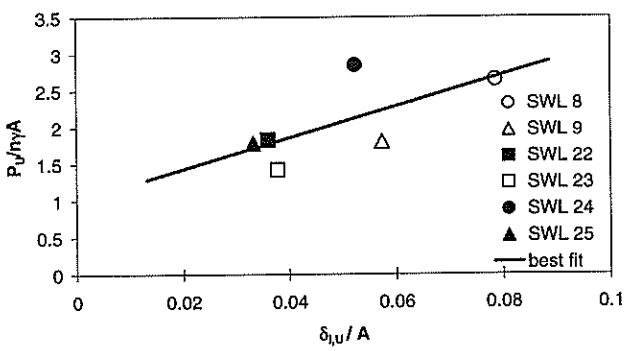

Fig. 25. Relationship between normalised ultimate uplift resistance $P_U/n\gamma A$ and injection thickness over depth $\delta_{i,U}/A$ for dense sand tests

The $\delta_{c,U}/D$ values for six dense sand centrifuge tests are plotted on Fig. 24 in terms of $\delta_{c,U}/D$ versus $P_U/[(n\gamma C)(1+Y/B)]$. A power curve fits the centrifuge data points very closely. The slope of the curve represents inverse shear modulus, as depicted in Equation (8), and it seems to increase. This is consistent with our understanding that stiffness reduces with shear strain represented by $\delta_{c,U}/D$. To find the effect of $\delta_{i,U}$ (injection thickness at ultimate uplift resistance point) on the maximum lining deformation, P_U in Equation (9) is transformed to $\delta_{i,U}$ using the relationship found from Fig. 25, where

$$P_U/n\gamma A = 1 + \alpha (\delta_{i,U} /A) \quad (10)$$

where α (=21.4) is the slope of the best-fit line in Fig. 25. Putting (10) into (9),

$$\frac{\delta_{c,U}}{D} \propto \frac{1 + \alpha\frac{\delta_{i,U}}{A}\frac{A}{C}}{(1+\frac{Y}{B})} \quad (11)$$

which leads to an injection geometry factor I_G,

$$\frac{\delta_{c,U}}{D} \propto I_G = \frac{A + \alpha\delta_{i,U}}{C} \frac{1}{(1+\frac{Y}{B})} \quad (12)$$

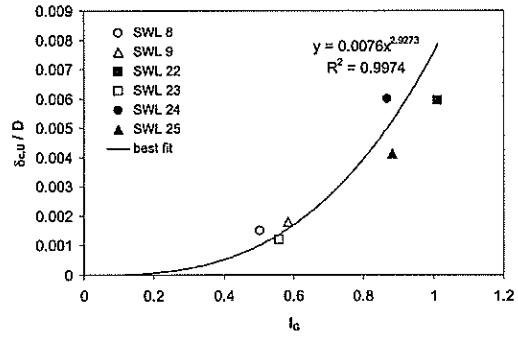

Fig. 26. Normalised maximum tunnel crow deformation $\delta_{c,u}/D$ versus injection geometry factor, I_G, for dense send tests

Figure 26 plots the centrifuge data for Equation (12) and it can be seen that the points again fall close to a power curve. The use of Fig. 26 to predict lining deformation during compensation grouting in the field would presently be unjustifiable owing to two main concerns: the correct scaling of deformations due to progressive soil rupture, and the significance of soil compressibility due to stress concentration around the individual ports of Tubes-a-Manchette. Nevertheless, Figs. 9, 24 and 26 offer strong guides to setting up properly normalised control groups within the scope of the Observation Method in the field.

MULTI-POINT SIMULTANEOUS INJECTION

Introduction

Three tests involving multi-point (three injectors) simultaneous symmetrical injection were carried out to compare their differences with strip injection, see Fig. 27. The main purpose is to investigate the effect of distributed grouting areas on lining deformation and ground movement. Table 2 details the tests configuration. In these tests, the valves connected to three injectors were opened simultaneously for the injection, see Fig. 2. The total injected volume to the three injectors, and the grouting pressure of each injector was recorded. It is assumed that the total injected volume has been distributed evenly to each injector. The side to side width (B') of the multi-point injectors was maintained at 80 mm for both types of injector widths, see Figs. 5 and 27.

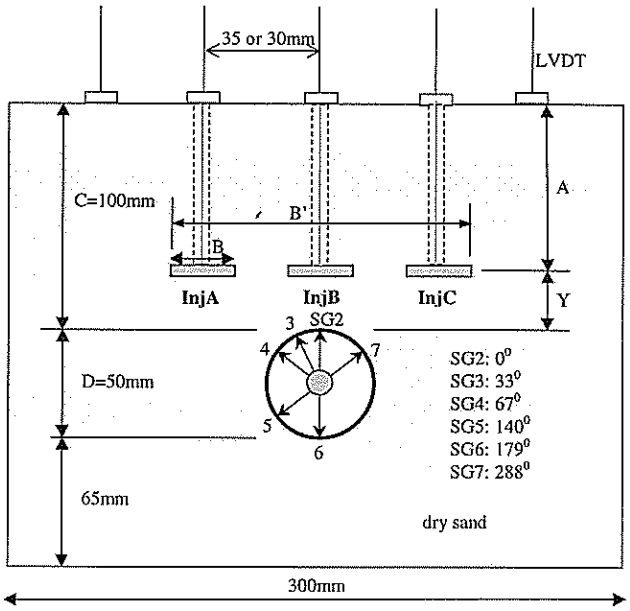

Fig. 27. Cross-sectional view of a multi-point injection injection model (not to scale)

Ground movement

Figure 28 shows an example (Test SWL 12) of the tests where the pressure increase is shown to be the same in each injector as the injection takes place. Figure 29 shows that the centre surface heaves can be assembled for tests in dense and loose sands (SWL 22, 12, 15 and 27) if plotted against the normalised grouting pressure to the power of η=mB/B', where B' is the total width of the array of m injectors each of width B. Exponent η represents the sparsity of injection within the grouted width, from 0 (intense injections with large gaps) to 1 (uniform injection as a strip). Test SWL 22 is a single strip injection test which has B' = 80 mm and η = 1; SWL 12 has η = 0.75 and SWL 15 and 27 have η = 0.375.

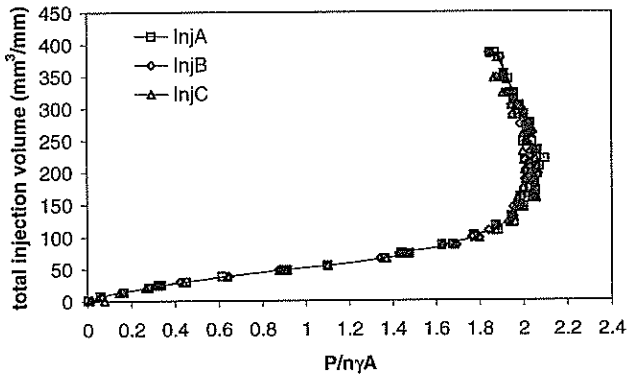

Fig. 28. Total injection volume vs. each injector normalised grouting pressure P/nγA test SWL 12

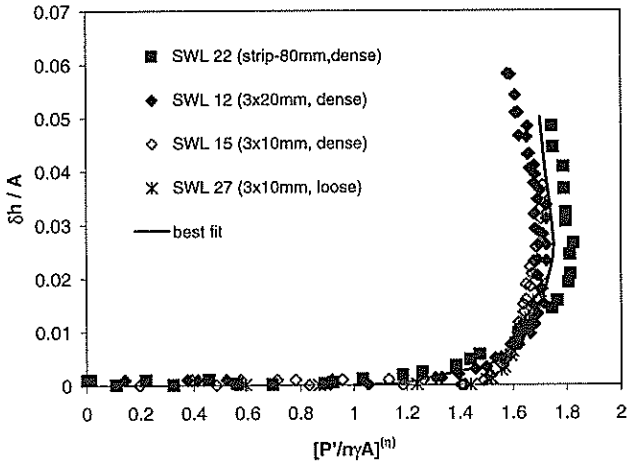

Fig. 29. Centre surface heave over injector depth ratio δh/A versus [P/nγA]$^{(\eta)}$

Figure 30 demonstrates the difference in centre surface heave over depth ratio δh/A between the strip and the multi-point injection tests when plotted against the normalised injection thickness δ_i'/B'. The parameter δ_i' is the total grout volume per total width of m injectors array (δ_i' = volume(ml) / *l*B'). Test SWL 15 (3 × 10mm) shows the highest centre surface heave followed by SWL 12 (3 × 20 mm), SWL 22 (strip-80 mm) and SWL 27 (loose-3 × 10 mm). Leaving gaps between injection points (smaller η value) is beneficial to the grouting efficiency for a certain δ_i'/B' value. Test SWL 27 (loose) shows half the δh/A value than test SWL 15 (dense) indicating that the compressive volume change of loose sand has suppressed the surface heave. Figure 31 illustrates the dilation and compression behaviour of dense and loose sand for tests SWL 15 and 27. Both tests show the same volume of compression until 80 mm^3/mm of injection volume. Thereafter test SWL 15 starts dilating while test SWL 27 continues showing compression but at a lower ratio than before.

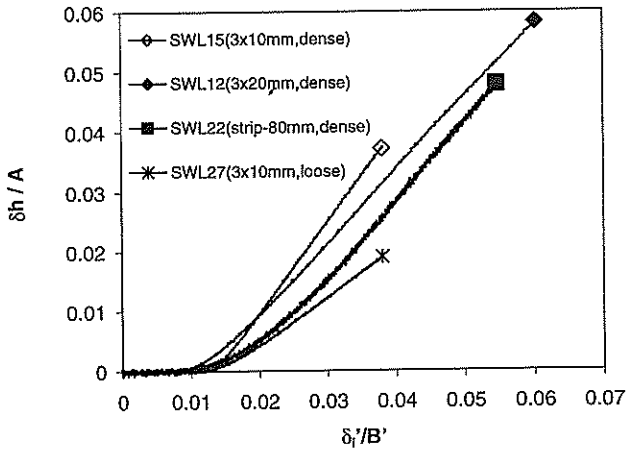

Fig. 30. Centre surface heave over injector depth ratio δh/A vs. normalised injection thickness δ_i'/B'

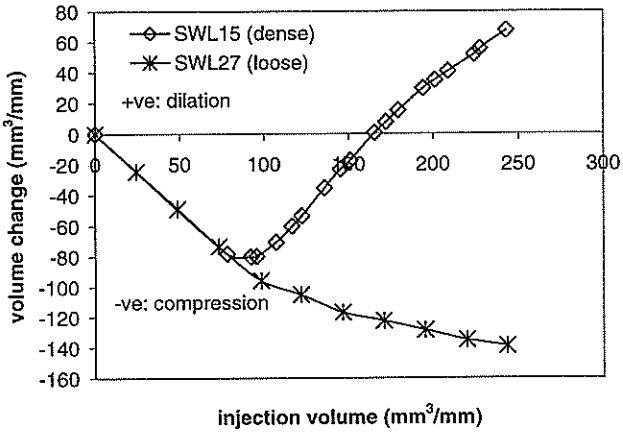

Fig. 31. Volume change vs. injection volume for tests SWL 15 (dense) & 27 (loose)

It is expected that in loose sand (SWL 27) some of the injector lift would have been absorbed by the compression behaviour of sand. Figure 32 substantiates this by showing that only 77% of the measured centre injector lift δ_{ih} was transmitted to the surface heave. In dense sand, the surface heave is initially equal to the injector lift. After overcoming P_U, sand dilation causes the heave to be more than the lift.

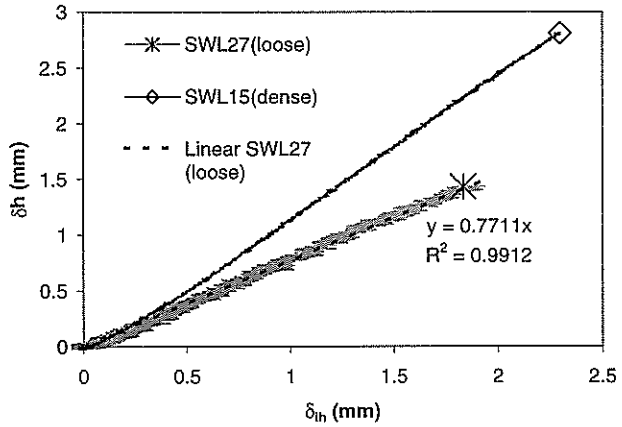

Fig. 32. Centre surface heave δh vs. centre injector lift δ_{ih} (SWL 15 & 27)

Lining deformation

The pattern of lining deformations is still the same as that with strip injection. In general, the tunnel crown and upper shoulder undergo inwards displacement, while the tunnel lower shoulder, haunch and invert experience outwards displacement. Figure 33 distinguishes the difference between the strip injection and the multi-point injection for normalised tunnel crown compression, δ_c/D with respect to normalised injection thickness δ_i'/B'. Test SWL 22 (strip- 80 mm) shows the largest δ_c/D followed by SWL 12 (3 × 20mm) and SWL 15 (3 × 10mm). Leaving gaps between the injectors (smaller η value) brings less effect to the lining deformation.

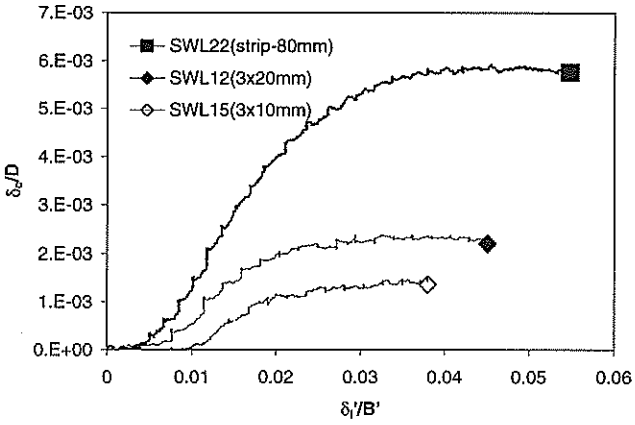

Fig. 33. Normalised tunnel crown deformation δ_c/D vs. normalised injection thickness δ_i'/B'

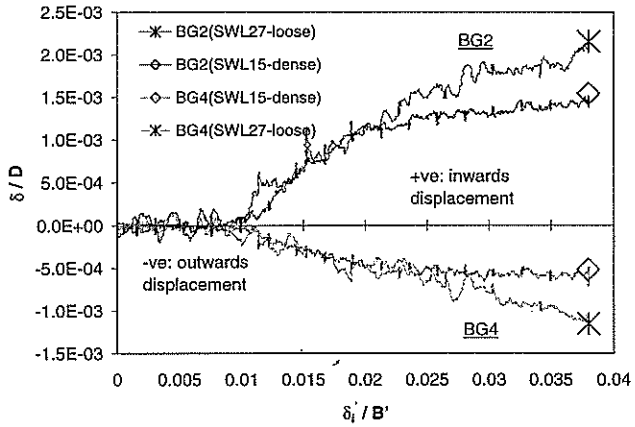

Fig. 34. Normalised tunnel lining deformation δ/D vs. normalised injection thickness δ_i'/B'(tests SWL 15-dense & 27-loose)

Figure 34 demonstrates the differences of lining deformations at tunnel crown (BG 2) and shoulder (BG 4) between test SWL15 (dense) and SWL 27 (loose) with respect to δ_i'/B'. Initially the lining deformations are almost the same regardless of sand conditions. Starting from δ_i'/B' ≈ 0.019, loose sand seems to give more lining deformation than dense sand. This is because of the more

surface heave experienced in dense sand at this stage where injection thickness pushes sand upwards and ceases to deform the lining. Figure 30 reveals that at $\delta_i'/B' \approx 0.019$ the centre surface heave in dense sand (SWL 15) is twice the value of loose sand (SWL 27). When those lining deformations are plotted against the grouting pressure, the same pattern of graph is observed, see Fig. 35. The loose sand curves begin forking away at P/nγA of 3.4. Referring to Fig. 36, starting from P/nγA of 3.4, the dense sand test (SWL 15) shows more heave than loose sand. The upward heave mechanism has mitigated the effect of grouting on the tunnel lining in dense sand.

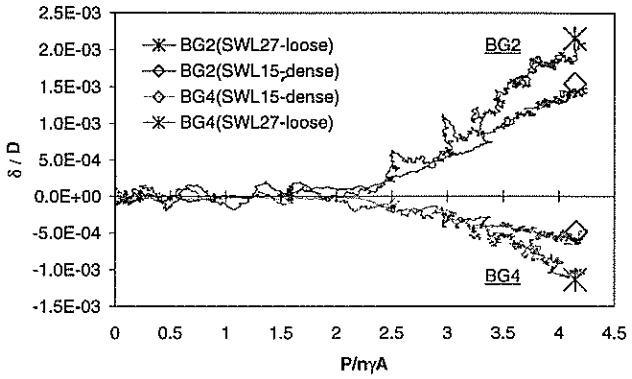

Fig. 35. Normalised tunnel lining deformation δ/D vs. normalised grouting pressure P/ηγA (tests SWL 15-dense & 27-loose)

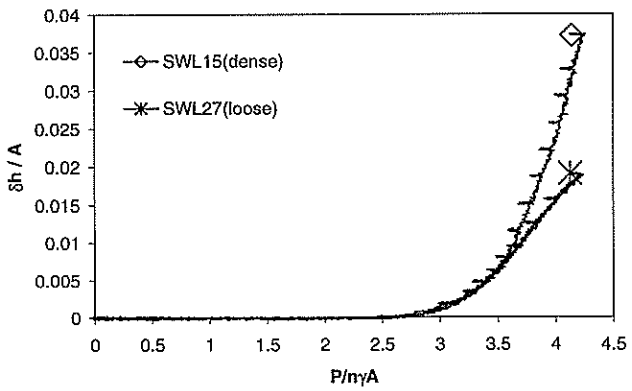

Fig. 36. Normalised centre surface heave δh/A vs. normalised grouting pressure P/nγA for tests SWL 15-dense and 27-loose)

DISCUSSION

The injection of grout into the ground above the crown of a tunnel, causing expansion of the surrounding ground, can lift the ground surface and can also deform the tunnel. This technique of compensation grouting requires sophisticated control of field operations, based on in situ displacement measurements. The chosen role for centrifuge model tests has been to vary injection geometries so as to arrive at certain dimensionless groups of parameters which should afford the field engineer a more fundamental basis for comparing the outcome of various patterns of grout injection. These dimensionless groups have been derived not simply from the blind application of Buckingham's theorem, but from mechanisms pertinent to the matter in hand. This will make it easier to relate the results to different soil types or injection patterns, for example.

The maximum possible pressure developed in a strip injection has been shown to relate simply to the break-out of the overlying block of soil, with considerations similar to the design of uplifting anchors. Equation (3) was shown to satisfy the test data quite accurately, in terms of dimensionless groups:

- P/(nγA), the ratio of injection pressure to the pre-existing overburden pressure;
- A/B, the injection strip depth/width ratio;
- K, an earth pressure coefficient which may be taken approximately as 0.67 based on the tests done in dense sand, and this value also seems reasonable for the single test in loose sand;
- tan ϕ, the internal friction of the soil at a pertinent density and stress.

These precepts are identical to those used in the design of pipelines against upheaval buckling, as is the magnitude of the dimensionless uplift pressure obtained at failure.

The mobilisation of shear stress on the sides of the uplifting block, versus its upward displacement, was normalised in a fashion similar to the skin friction on piles, using a mobilised shear coefficient $\beta = K \tan \phi$ versus a normalised soil displacement δh/A. The ultimate mobilisation at $\delta h/A \approx 0.02$-0.03 of $\beta_{ult} \approx 0.8$ for dense sand, and at $\delta h/A \approx 0.06$ of $\beta_{ult} \approx 0.45$ for loose sand are quite consistent with design practice for shallow piles and piers, as is the hyperbolic shape of the mobilisation curve.

The deformation of the tunnel lining, as a result of injection, was described in Equation (9) in terms of the following dimensionless groups based on a simplified mechanism:

- δ_c/D, the proportional tunnel crown distortion,
- P/(nγC), the ratio of injection pressure to tunnel overburden (representing sand stiffness),
- B/(B + Y), the ratio of injection width to the width of tunnel influenced at its crown.

The maximum deformation was expected, and found, to occur at the maximum injection pressure, and by assuming that the injection volume at failure would be proportional to the failure pressure, a further simplification in Equation (12) was able successfully to link tunnel deformation with injection geometry, using a power curve.

Further tests investigating the effect of separate injections over a given width, in comparison to a single strip injection, were nicely organised by using the sparseness η of the injections as an exponent on the normalised injection pressure, taking the lesson that power curves seem to fit much of the present data.

The mechanisms used to organise the centrifuge data might look familiar and even obvious in retrospect, but could not have been recommended confidently in the absence of model data. The dimensionless charts and normalisations should make it easier for field monitoring data to be assembled in the most meaningful way. Equally, however, there are sufficient dissimilarities between field and model injection sequences to caution the field engineer against the blind application of the actual numerical values of the dimensionless parameters derived above. In particular, field injections are not simultaneous over a current zone of grouting, are more sparse, and their distribution is 3-dimensional rather than in plane strain. These concerns currently being addressed through further model tests and matching finite element analyses.

It might be argued that the introduction of a copper strip injector alters the local stiffness of the ground not only after injection (as occurs with the creation of cement bodies in the ground) but also before injection starts. Ideally, real grout injection would have been made from scaled TAM tubes (0.7mm diameter at model scale), and the grout itself would have displaced the surrounding soil. The impossibility of delivering this ideal lead to the adoption of the experimental strip injector which has been used here to advance our knowledge on the effect of injection near tunnel linings. Of course, this is far from saying that the injection technique which had been used was fully representative of TAM grouting in the field.

CONCLUSIONS

1. The limiting injection pressures in the model tests were related to the drag down of a soil block projected vertically above the area of injection, rather as though the pull-out capacity of a tension pile were being calculated. The maximum shear coefficient β was 0.8 ± 0.2 for dense sand mobilised at a lift ratio $\delta h/A \approx 0.02$-0.03, and 0.45 for loose sand mobilised at a lift ratio of 0.06.
2. Grout efficiency in terms of heave volume produced per unit of injection volume within a strip zone was reduced towards 50% in loose sand, or when the injection pressure was high because the injection width / depth was small and the pressure relaxation was sustained over long periods. Efficiencies greater than unity could be observed in dense sand with wide injection zones, where global dilatancy exceeded local compression.
3. It was suggested that the controlling influence on tunnel distortion might be the injection geometry factor I_G. In the model tests the proportional crown depression $\delta_{c,U}/D$ approached 0.6% as I_G passed 0.9. It was found in the strip injection tests that $\delta_{c,U}/D$ increased roughly as the third power of I_G.
4. Where injections were made at intervals within a given strip width, it was found that the influence of their sparseness η on the heave measured on the ground surface could be introduced directly as an exponent η on the normalised injection pressure $P/\eta\gamma A$. In this way it could be seen that sparse injections generated high injection pressures, but that grout efficiency was improved while tunnel distortion was significantly reduced.

ACKNOWLEDGEMENT

The authors wish to gratefully acknowledge the financial support provided by the Nishimatsu Construction Co. Ltd., Tokyo, and the technical contributions from the technicians of the Schofield Centrifuge Centre.

REFERENCES

1) Baker, W.H., Cording, E.J. and Macpherson, H.H. (1983): "Compaction grouting to control ground movements during tunnelling," Underground space, Vol.7, pp. 205-212.
2) Bolton, M.D., (1986) : "The strength and dilatancy of sands," Geotechnique, 36, No.1, pp. 65-78.
3) Bolton, M.D., (1987) : "Discussion on The strength and dilatancy of sands," Geotechnique, 37, No. 2, pp. 219-226.
4) Brown, D.R. and Warner, J. (1973): "Compaction grouting," Journal of the Soil Mechanics and Foundation Division, ASCE, Vol. 99, No.SM 8, Proc. Paper 9908, pp. 589-601.
5) Drooff, E.R., Tavares, P.D. and Forbes, J. (1995): "Soil fracture grouting to remediate settlement due to soft ground tunnelling," Proc. Rapid Excavation and Tunnelling Conf., San Francisco, pp. 21-40.
6) Harris, D.I., Mair, R.J., Love, J.P., Taylor, R.N., and Henderson, T.O. (1994): "Observation of ground and structure movements for compensation grouting during tunnel construction at Waterloo Station," Geotechnique, 44, No. 4, pp. 691-713.
7) Kovacevic, N., Edmonds, H.E., Mair, R.J., Higgins, K.G. and Potts, D.M. (1996): "Numerical modelling of the NATM and compensation grouting trials at Redcross Way," Prof. Int. Conf. on Geotechnical Aspects of Underground Construction in Soft Ground, Mair R.J. and Taylor R.N. (eds), London, Balkema, pp. 553-559.
8) Lee, S.W., Dasari, G.R., Mair, R.J., Bolton, M.D., Soga, K., Sugiyama, T., Ano, Y., Hagiwara, T. and Nomoto, M. (1999): "The effects of compensation grouting on segmental tunnel linings," Proc. Geotechnical Aspects of Underground Construction in Soft Ground, Tokyo, pp. 257-262.
9) Linney, L.F. and Essler, R.D. (1994): "Compensation grouting trial works at Redcross Way, London," Grouting in the Ground, Thomas Telford, London, pp. 313-326.
10) Mair, R.J. and Hight, D. (1994): "Compensation grouting," World Tunnelling Review, November, pp. 361-367.
11) Mitchell, J.K. (1992): "Fundamentals of soil behaviour," Second edition, John Wiley & Sons, Inc., p. 342.

12) Nicholson, D.P., Gammage, C. and Chapman, T. (1994): "The use of finite element methods to model compensation grouting," Grouting in the Ground, Thomas Telford, London, pp. 297-312.

13) Peck, R.B.(1969): "Deep excavation and tunnelling in soft ground," State-of-the-art-report, 7th Int. Conf. In Soil Mechanics and Foundation Engineering, Mexico City, pp. 225-290.

14) Rubright, R. and Welsh, J. (1993): Ground Improvement, Edited by M.P.Moseley, Blackie Academic & Professional, pp. 131-148.

15) Schweiger, H.F. and Falk, E. (1998): "Reduction of settlements by compensation grouting - Numerical studies and experience from Lisbon underground," Tunnel and Metropolis, Negro J.R. and Ferreira (eds), Balkema, pp. 1047-1052.

16) Tan, F.S.C. (1990): "Centrifuge and theoretical modelling of conical footings on sand," PhD thesis, Cambridge University.

17) Zeigler, E.J. and Wirth, J.L. (1982): "Soil stabilisation by grouting on Baltimore Subway," Proc. of Conf. on Grouting in Geotechnical Engineering, New Orleans. ASCE, pp. 576-590.